Continental Shelf Research 230 (2021) 104558

Contents lists available at ScienceDirect

Continental Shelf Research

journal homepage: www.elsevier.com/locate/csr

Physical mechanisms driving biological accumulation in surface lines on coastal Hawaiian waters

Katharine A. Smith [a,b,*], Jonathan L. Whitney [a,b,c], Margret A. McManus [a], Joey Lecky [c,d], Adrienne Copeland [e], Donald R. Kobayashi [c], Jamison M. Gove [c]

[a] Department of Oceanography, University of Hawai'i at Mānoa, Honolulu, HI, 96822, USA
[b] Joint Institute for Marine and Atmospheric Research, University of Hawai'i at Mānoa, Honolulu, HI, 96822, USA
[c] Pacific Islands Fisheries Science Center, National Oceanic and Atmospheric Administration, Honolulu, HI, 96818, USA
[d] Lynker, LLC, Leesburg, VA, 20175, USA
[e] Office of Ocean Exploration and Research, National Oceanic and Atmospheric Administration, Silver Spring, MD, 20910, USA

ARTICLE INFO

Keywords:
Internal wave slicks
Internal waves
Submarine groundwater discharge
Surface slicks
Marine ecosystems

ABSTRACT

Lines of smooth ocean surface water known as "slicks" appear in coastal waters worldwide and can be caused by a number of natural mechanisms. Off the western coast of the island of Hawai'i, USA, internal waves, submarine groundwater discharge, tidal fronts, and headland fronts were all observed to cause the formation of slicks. Neuston net sampling showed slicks to contain enhanced densities of phytoplankton, zooplankton, larval invertebrates, larval fish, and plastic fragments when compared to ambient water. In particular, internal wave slicks were observed to be both the most frequently occurring type of slick and the overall strongest accumulator of neustonic organisms and plastics when compared to the other types of slicks. Satellite imagery illustrated that slicks are visible along most of the West Hawai'i coastline more than 75% of the time. Furthermore, acoustic backscatter observations showed that the accumulation associated with slicks frequently extended from the surface to depths of 5 m. These findings highlight the important roles internal wave slicks can have in coastal ecosystems.

1. Introduction

Long, meandering lines of smooth surface water, sometimes referred to collectively as "slicks," can be seen in coastal waters around the world (e.g., da Silva et al., 1998; Hsu et al., 2000; Munk et al., 2000; Ryan et al., 2010). These lines, whose smooth appearance results from the suppression of small ripples, can be caused by a number of physical mechanisms, including internal waves (Curtin and Mooers, 1975; Shanks, 1983) and fronts (Ryan et al., 2010; Woodson et al., 2012). Slicks have been observed to be hotspots of biological accumulation, making them potentially important components of the ecosystems where they are present (e.g., Gove et al., 2019; Kingsford et al., 1991; Ryan et al., 2010; Shanks, 1983; Whitney et al., 2021). Slicks have also been observed to accumulate plastic debris (Gove et al., 2019; Young and Adams, 2010), raising concerns about the potential for increased interactions between microplastics and marine organisms in slicks.

Linear internal waves cause alternating regions of divergent and convergent surface currents that may result in parallel bands of slicks perpendicular to the direction of wave propagation (Ewing, 1950; Lafond, 1959) (see Supplemental Fig. S1). These internal wave slicks have been observed to accumulate algae (Franks, 1997), zooplankton (Mattos and Mujica, 2012), larval invertebrates (Shanks 1983, 1995; Weidberg et al., 2014), and larval fish (Kingsford and Choat, 1986; Shanks, 1983), and they have also been observed to transport materials (e.g., Franks et al., 2020; Shanks, 1983). Internal waves can additionally create slicks through nonlinear behavior, as an internal wave bore shoaling on a topographic slope can set up a surface warm front that propagates shoreward (Pineda, 1994). Fronts caused by internal wave bores in this way have been observed to transport neustonic larvae (Pineda, 1991, 1994).

Other types of fronts have been found to accumulate organisms in slicks, whether because of convergent currents or organism behavior (Roughgarden et al., 1991; Woodson and McManus, 2007). Accumulations of zooplankton, larval invertebrates, and larval fish have been observed in tidal fronts (Kingsford et al., 1991), upwelling fronts (Roughgarden et al., 1991; Woodson et al., 2012), outflow plume fronts

* Corresponding author. Department of Oceanography, University of Hawai'i at Mānoa, Honolulu, HI, 96822, USA.
E-mail address: kasmith6@hawaii.edu (K.A. Smith).

https://doi.org/10.1016/j.csr.2021.104558
Received 21 September 2020; Received in revised form 13 September 2021; Accepted 14 September 2021
Available online 20 September 2021

(Kingsford, 1990), and headland fronts (Morgan et al., 2011) (see Supplemental Fig. S2).

Previous studies have examined slicks using field observations (e.g., Kingsford et al., 1991; Pineda, 1991; Shanks, 1983) and satellite imagery, such as Synthetic Aperture Radar (SAR) (e.g., da Silva et al., 1998; DiGiacomo and Holt, 2001; Marmorino et al., 2008; Ryan et al., 2010). SAR images show surface roughness, making them well suited for imaging slicks, and have the advantage of capturing surface imagery regardless of cloud cover. One factor that can affect slick observation, whether *in situ* or via SAR, is wind. If winds are too weak (<2–3 m s^{-1}), the ocean surface appears smooth, while if winds are too strong (>7–10 m s^{-1}), the ocean surface appears rough, regardless of the presence or absence of slicks (Holt, 2004).

Most studies on the ecosystem effects of slicks have been in temperate continental shelf regions (e.g., Mattos and Mujica, 2012; Pineda, 1991; Shanks, 1983; Weidberg et al., 2014; Woodson and McManus, 2007; Woodson et al., 2012), though a few have been in tropical regions (Kingsford et al., 1991; Leichter et al., 1998). Leichter et al. (1998) found increased concentrations of zooplankton, fish larvae, and invertebrate larvae associated with internal wave bores in a Florida Keys (USA) coral reef, but these were only subsurface observations. Kingsford et al. (1991) found accumulations of zooplankton and pre-settlement fishes in tidal fronts in a section of the Great Barrier Reef. Both studies focused on shallow water observations at isobaths <50 m on continental shelves, and neither study observed internal wave slicks. Islands in oligotrophic, tropical oceans can create habitats rich in phytoplankton biomass, supporting abundant coral reef ecosystems and higher trophic levels (Gove et al., 2016). Furthermore, persistent stratification in the tropics is conducive to shallow-water internal waves and may allow slicks to be prevalent in coastal ecosystems throughout the year.

Slicks are a common feature off the west coast of the island of Hawai‘i (Hawai‘i, USA), the largest and southeasternmost island in the Hawaiian archipelago (Fig. 1). The Hawaiian Ridge is a site of strong internal wave generation, as tidal currents periodically force stratified currents over steep underwater topography (Merrifield and Holloway, 2002; Rudnick et al., 2003). The west side of the island of Hawai‘i (hereafter West Hawai‘i) does not have significant river systems (Kay et al., 1977), but submarine groundwater discharge (SGD) creates brackish discharge plumes visible in coastal waters (Johnson et al., 2008; Peterson et al., 2007). Northeasterly trade winds dominate the regional wind patterns, putting West Hawai‘i in the lee of the island's two >4000 m tall shield volcanoes. A notable characteristic of the island is its steep southwest slope, where water depths of 1000 m are found closer than 2 km from shore. The northwest slope is gentle by comparison, descending to the 1000 m isobath 15 km or more from the coastline. The shallow waters along the western shelf of the island are dominated by coral reefs. Because the steep bathymetry acts to compress the shelf and slope ecosystems, larvae of coral reef, epipelagic, mesopelagic, and even benthopelagic fishes can all be found in the island's nearshore waters (Reid et al., 1991).

The rich, diverse marine ecosystem of West Hawai‘i, along with the presence of multiple slick-forming mechanisms and wind conditions favorable for slick observation, made it a prime location to investigate the accumulation of various organisms in slicks. The overarching goal of this study was to quantify patterns of accumulation of phytoplankton, zooplankton, larval invertebrates, and larval fish in slicks. Two other publications based on the same field study, Gove et al., (2019) and Whitney et al. (2021), explore the accumulative effects of slicks. The former focuses on the relationship between larval fish and plastic debris that are concentrated in slicks, while the latter explores in detail the ecological role of slicks as larval fish nurseries and how accumulation varies among species and life stages. In this contribution, our field observations provide insights into the different mechanisms driving slicks, the variability in accumulation among slicks, and effects of slicks on various ecosystem components. In addition, satellite data allow us to increase the spatial and temporal scales of slick observations and characterize conditions under which they form. Ultimately, this work provides critical insights into the underlying physical drivers of slicks and their role in enhancing tropical island ecosystems.

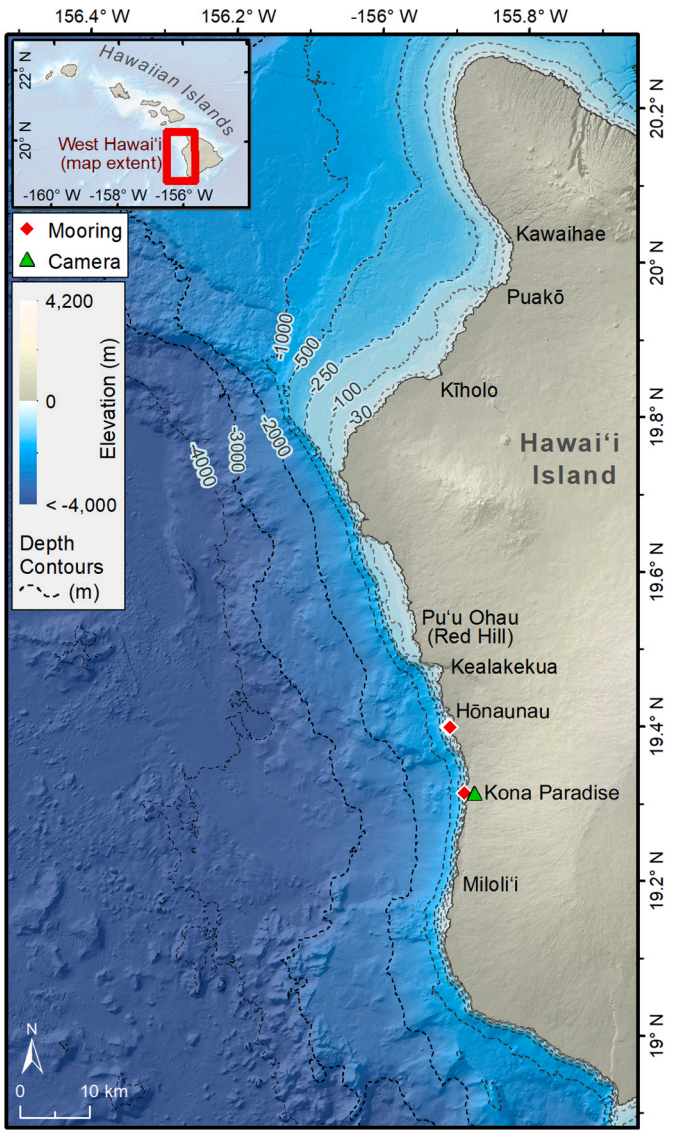

Fig. 1. Map of study region, with relevant locales marked. Mooring locations are marked as red diamonds; the time-lapse camera location is marked as a green triangle.

2. Methods

2.1. Field study

Three field expeditions were conducted (September 6–25, 2016; April 17–May 1, 2017; and July 10–19, 2018) offshore of West Hawai‘i (Fig. 1), as part of the National Oceanic and Atmospheric Administration's West Hawai‘i Integrated Ecosystem Assessment (West Hawai‘i IEA), a research program dedicated to understanding marine ecosystem dynamics in the region. Slick surveys were conducted from NOAA Ship *Oscar Elton Sette* as well as several small boats deployed either from shore or from the *Sette*. Additionally, oceanographic moorings were deployed during the field expeditions.

2.1.1. Surveys

Slick surveys were conducted primarily using small boats. All three expeditions had one boat dedicated to collecting net samples. The September 2016 expedition had an additional boat for collecting acoustics (backscatter) and CTD (conductivity, temperature, depth) data, while the April 2017 field expedition had an additional boat for slick mapping. The small boats surveyed slicks at locations within 6.5 km of the shoreline over depths from 12 to 1300 m, between the hours of 8:00 a.m. and 4:00 p.m. local Hawai'i Standard Time (HST, UTC -10). Slicks were identified and selected visually from the small boats to fit the criteria of being at least 1 km in length and clearly distinguishable from surrounding non-slick waters. The team was particularly interested in surveying internal wave slicks, but a number of slicks were sampled that were later classified as being caused by other mechanisms (i.e., tidal fronts, headland fronts, or groundwater discharge).

The acoustics boat was equipped with a calibrated Simrad EK60 200 kHz scientific echosounder mounted on the end of a pole pointing downward ~1 m below the surface. The pulse duration and power were set to 512 μs and 150 W, respectively. The echosounder was calibrated using a 38.1 mm diameter tungsten-carbide reference sphere and standard techniques (Foote et al., 1987; Demer et al., 2015). The echosounder recorded data from about 2 m to 280 m below the surface. A Sea-Bird Electronics SBE 19plus SeaCAT Profiler Conductivity-Temperature-Depth (CTD) instrument was hand-cast from the acoustics boat from 1 to 12 m depth, recording in 1 m bins and sampling at 1 Hz (~2–3 samples per bin).

The survey of each slick began at the approximate length-wise midpoint of the slick (Fig. 2), where three CTD casts were conducted: one inside and two a few meters outside either edge of the slick. The boat then conducted a transect at a speed of ~2.5 knots along the central axis of the slick away from the midpoint, either until 500 m was traveled or until reaching the end of the visible slick (whichever was shorter). The boat then moved outside of the slick and conducted a similar 500 m transect in the reverse direction outside of and parallel to the slick, taking a single "ambient water" CTD cast at the beginning of this transect. The mean distance between the centroids of slick/ambient transect pairs was 217 m. Acoustic backscatter was logged continuously throughout the surveys at a sampling period of ~0.7–1.4 s, dependent on the water depth. A total of 36 slicks with paired ambient-water samples were surveyed by the acoustics boat in 2016.

Additionally, surface water samples were collected at a subset of slick and ambient transects (n = 39 each) to determine concentrations of chlorophyll. Samples for chlorophyll were collected by hand using 1 L or 150 mL dark Nalgene bottles and immediately placed on ice in the field. Water samples were later filtered onto 25 mm GF/F glass microfiber filters (Whatman), placed in 10 mL of 90% acetone, frozen for 24 h, and then analyzed for chlorophyll *a* with a Turner Designs model 10AU field fluorometer.

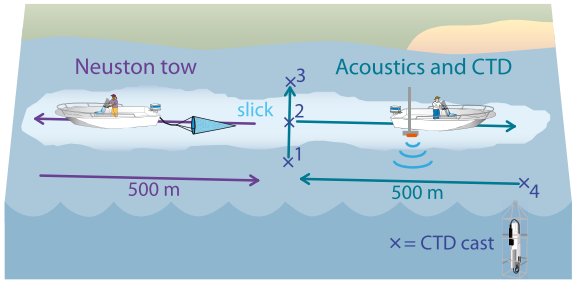

Fig. 2. Diagram of slick sampling protocol. Boat with neuston net started near the center of the slick and conducted an in-slick tow in the along-slick direction for 500 m, then conducted a parallel 500 m tow in nearby ambient waters. Boat with acoustics and CTD started near the center of the slick and conducted CTD casts in sequence just outside one edge, in the middle, and just outside the other edge of the slick. It then proceeded for 500 m in the along-slick direction opposite from the neuston boat, conducted another CTD cast in ambient water, then proceeded 500 m parallel to the slick in ambient water.

The net sampling boat used a 1 m diameter conical neuston net (335 μm mesh, 4.5 m length, Sea-Gear Corp.) to conduct surface tows from the air-water interface to ~1 m depth. The neuston net design was based on the manta net (Brown and Cheng, 1981) and is described in detail in Gove et al., (2019) and Whitney et al. (2021). The net was towed using an asymmetrical bridle and paravane to ensure the net frame was clear of the towing vessel's wake. The surface net was fitted with a 300 μm mesh soft cod end and a mechanical flowmeter (Sea-Gear Corp, mouth area = 0.79 m^2). The total water volume sampled for each tow was calculated by multiplying the flow through the meter by the mouth area of the net.

The boat began each of its neuston tows at the length-wise midpoint of the slick but proceeded along the central axis in the direction opposite that of the acoustics boat (Fig. 2). Neuston tows were conducted at a speed of ~2.5 knots for either ~8 min or until reaching the end of the visible slick (whichever was shorter). Tow length was 495 ± 157 m (mean ± s.d.). Similar transects were conducted in parallel lines in ambient water outside of the slicks but were not always paired 1:1; generally, one ambient tow was used as a baseline for several nearby slick tows. "Primary pairs," defined as an ambient transect paired with only the nearest inside-slick transect, were highlighted in some of our analyses. The small net sampling boats surveyed a total of 70 slicks, with 46 considered to be a primary pair with an ambient tow. Considering all pairs of slick and ambient transects (not just primary pairs), the average distance between members of each pair was 1.2 km. See Gove et al., (2019) for full details on the net sampling techniques.

In 2017, neuston tows were conducted for 10 slicks from the *Oscar Elton Sette*, using a similar process to that conducted from the small boat. A 1.8 m (6 ft) Isaacs-Kidd (IK) trawl (Isaacs 1953; Aron 1962) equipped with a winged depressor and 505 μm mesh was deployed alongside to mitigate disturbance from the ship, sampling from slightly above the air-sea interface down to ~1.5 m depth. The IK trawl was fitted with a mechanical flowmeter (Sea-Gear Corporation) mounted in the mouth of the net (mouth area = 2.75 m^2) providing the total volume sampled for each tow. Neuston tows were conducted for ~12 min at a speed of ~3.5 knots. Tow length for IK neuston tows conducted from the ship was 1012 ± 356 m (mean ± s.d.).

GPS mapping was the primary goal of the third small boat used in April 2017, as it attempted to travel the full extent of each slick to provide a quantification of the spatial dimensions of the slicks. All small boats were equipped with a Garmin GPSMap 78 handheld GPS unit, which logged location continuously (accuracy ≤10 m).

A drifter equipped with a Nortek 2 MHz Aquadopp current profiler was deployed during the July 2018 surveys. This drifter was designed following the methods of Mullarney and Henderson (2013): the 2 MHz Aquadopp with right-angle transducer head was attached to a square frame of PVC pipe to face downward at approximately 0.15 m depth as the drifter floated at the surface, with a Garmin GPSMap 78 (logging continuously) attached to the upper side of the drifter frame. The Aquadopp was set with a blanking distance of 0.1 m and a bin size of 0.25 m over a total of 5 m in order to profile with high vertical resolution very near to the surface. The Aquadopp recorded mean currents over 30-s intervals, but its primary use was for backscatter counts. The drifter was deployed inside a slick and allowed to drift for 20–30 min; in some cases, it exited the slick, while in others it drifted inside the slick for the entire deployment. Six slicks sampled with the neuston tows were surveyed by the drifter.

As the slicks were surveyed in the field, detailed characteristics of the slick and environment were recorded in field notes. These included the estimated width of the slick, the visual contrast between the slick and ambient water, slick alignment with the shoreline and propagation direction, other notable features in appearance (visible algal accumulation, etc.), nearest neighboring slick distance and direction, and wind conditions. These detailed notes were taken into consideration when the

mechanism for each individual slick was determined (see section 2.3).

2.1.2. Moorings

A mooring was deployed from 17 to 24 September 2016 south of Hōnaunau (155.91257°W, 19.40073°N; Fig. 1) at 36 m depth, which included nine temperature sensors distributed between 1.5 m and 33 m above bottom. Another mooring was deployed from 21 to 29 April 2017 offshore of Kona Paradise (155.89093°W, 19.31522°N; Fig. 1) at 38 m depth, which included eight temperature sensors distributed between 5 m and 32 m above bottom. The temperature sensors were an assortment of SBE39 and SBE56 sensors (Sea-Bird Scientific), including an SBE39 with both temperature and pressure sensors at the topmost positions. The mooring deployed in 2017 included an upward-looking 300 kHz Nortek Acoustic Doppler Current Profiler (ADCP), positioned with its head at 3 m above bottom and programmed with a blanking distance of 88 cm and a bin size of 2 m.

2.2. Remotely sensed data

Sentinel-1 SAR images (courtesy of European Space Agency, Copernicus Program) of West Hawai'i were accessed and visualized via Google Earth Engine (Image Collection: COPERNICUS/S1_GRD) (Gorelick et al., 2017). There were 225 unique dates with SAR imagery of the region between November 7, 2014 and March 27, 2018. These images were captured at either 4:30 UTC (ascending passes) or 16:15 UTC (descending passes) (6:30 p.m. or 6:15 a.m. HST, respectively), with intervals between images ranging from 2.5 days to 14.5 days. The SAR images show surface roughness, with lighter shades representing rougher surfaces (higher backscatter) and darker shades representing smoother surfaces (lower backscatter) (see Fig. 3A). In general, the ocean appears dark compared to the largely white land surface, but shades of gray show differences in the ocean roughness. Slick lines appear in the images as long, narrow, dark bands; such bands can be indicative of internal waves, headland fronts, eddy fronts, and other features that lead to bands of smooth water or biogenic oils (substances released or exuded by marine organisms), which can suppress surface ripples (Holt, 2004).

Wind speed and direction were obtained from the Pacific Islands Ocean Observing System (PacIOOS) Weather Research and Forecasting (WRF; 6 km resolution) model of the main Hawaiian Islands (http://www.pacioos.hawaii.edu/weather/model-wind-hawaii/). Tidal heights and currents were obtained using the TPXO8-atlas (http://volkov.oce.orst.edu/tides/tpxo8_atlas.html) at 1/6° resolution and processed using the TMD Matlab Toolbox (https://www.esr.org/research/polar-tide-models/tmd-software/).

2.3. Mechanism determination

Each slick surveyed in the field study (Section 2.1.1) was categorized according to its most probable generating mechanism, considering all field observations and available supplementary data. These data included the GPS mapping of the surveyed slicks, field notes (e.g., direction of propagation, distance and alignment of nearest neighbor slicks), wind conditions (as noted in the field and as seen in WRF), tidal phase (as derived from TPXO8), SGD from Johnson (2008), bathymetry (HMRG 50 m multibeam bathymetry synthesis, http://www.soest.

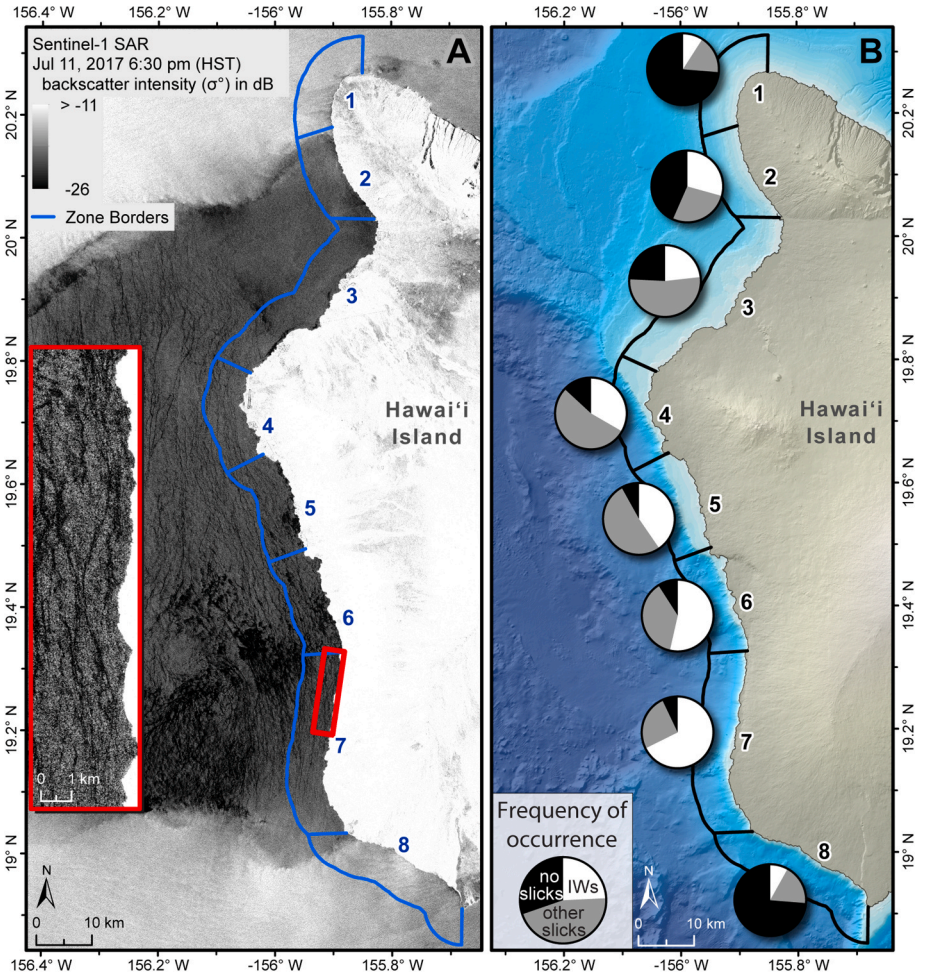

Fig. 3. (A) Example of SAR imagery of West Hawai'i island region from July 11, 2017 at 6:30 p.m. HST. Slicks appear as dark streaks on the water, while water roughness caused by high winds is visible in the northern and southern regions of the image. Blue lines mark the borders of the zones used for the SAR analysis (Section 2.4.3). (B) Pie charts indicate frequency of the presence of internal wave (IW) slicks (white), slicks other than internal wave slicks (gray), and the presence of no slicks (black) per zone, as observed from 225 SAR images collected during 2014–2018. Zones are numbered and outlined in black.

hawaii.edu/HMRG/multibeam/index.php), SAR imagery, images from Landsat 8 (USGS, https://www.usgs.gov/land-resources/nli/landsat) and Sentinel-2 (European Space Agency, https://earth.esa.int/web/sentinel/user-guides/sentinel-2-msi/product-types/level-1c), persistence, and distance from shore. The slick-generating mechanisms identified included internal wave slicks, SGD fronts, tidal fronts, and headland fronts.

Characteristics that indicated an internal wave slick were the presence of multiple lines in parallel spaced approximately 50–200 m apart, alignment parallel to isobaths, and propagation onshore (as recorded in field notes) and in the direction perpendicular to the slick's alignment (determined from GPS and field notes). Slicks close to land (especially perpendicular to shore) that were noted in the field notes as being stationary were compared to maps of SGD in Johnson (2008) to determine the likelihood of their source being SGD. Tidal fronts were identified as persistent, solitary, stationary lines parallel to shore in the 130 m–200 m depth range, taking into account the tidal phase. Tidal phase was based off of TPXO tidal heights, which were found to be accurate in relation to the K1 mooring, with high tide corresponding to southward flow and low tide corresponding to northward flow at the mooring (correlation of -0.56, p-value<0.01). Lastly, stationary slicks located near headlands and not associated with the location of known SGD outflows were determined to be probable headland-associated fronts, again considering likely tidal current based on TPXO tidal height.

2.4. Data analysis

2.4.1. Sample processing

Organisms and plastics were identified under a dissecting microscope and manually sorted into key groups: invertebrate zooplankton, fish larvae, and plastics. Invertebrate zooplankton samples were enumerated and identified into broad taxonomic groups and life stages when possible; in the analysis of this study, the subcategories of larval invertebrates (e.g., crabs, shrimp, gastropods) and zooplankton were distinguished. Methods for plastic identification followed procedures outlined in Gove et al., (2019). In short, plastics manually extracted from each sample were dried, weighed, and photographed using a high-resolution camera (Nikon D7000) and analyzed using ImageJ (Schneider et al., 2012) to provide the total number of plastic particles per tow. All counts (zooplankton, larval invertebrates, larval fish, plastics) were standardized to the volume of water sampled for each tow and converted to densities (total number m^{-3}).

Densities from each slick transect were divided by the corresponding densities from the nearest ambient transect to calculate a "concentration factor" for each slick, essentially representing how many times more concentrated each category of specimen was inside the slick than outside the slick. Chlorophyll *a* concentration from the water samples were similarly compared with ratios between slick and ambient values to calculate their concentration factors. Concentration factors for each slick were sorted by the most probable mechanism generating the slick, and the mean and standard error for the concentration factors were calculated for each mechanism.

2.4.2. CTD and acoustics

Data from the CTD casts were averaged into 1 m depth bins. Upcasts of the SBE 19plus CTD were used for the CTD temperature profiles because of a delay in the pump start time. Fine structure may be disrupted when upcasts are used instead of downcasts, but at the resolution of 1 m depth bins, the effect was likely negligible.

Acoustics backscatter data from the calibrated Simrad EK60 200 kHz echosounder were available for 23 slicks. Noise and missing data were excluded in ECHOVIEW 8.0 (Echoview Software Pty. Ltd, 2017) using standard cleaning techniques (De Robertis and Higginbottom, 2007). Data shallower than 3 m in depth were removed to avoid interference due to the instrument. The data were binned into cells with 1 m horizontal resolution and 1 m vertical resolution. The cells were integrated and the dB mean volume backscattering strengths (Sv; units: dB re 1 m^{-1}), a proxy for relative density of sound-scattering particles per unit volume (Simmonds and MacLennan, 2005), were extracted. Backscatter over the course of the along-slick or ambient transects were averaged over time, by depth bin, for the course of that transect. Backscatter values were converted from the log-scale Sv units to the linear scale before calculating the ratio between mean slick and ambient backscatter.

For the Nortek Aquadopp attached to the drifter, echo intensity data were used to estimate the backscattering strengths (Sv; dB re 1 m^{-1}) following Deines (1999). Based on the Rayleigh distance for the instrument (Mullison, 2017), we estimated that only data more than 0.5 m from the transducer head were useable. The two bins closest to the instrument were therefore excluded; the first bin used started at a distance of 0.725 m from the instrument.

2.4.3. SAR images

The SAR images of the region were analyzed for simple presence or absence of slick lines to obtain basic quantitative information over space and time. To do this, the coastal waters up to 6.5 km from shore (the maximum offshore distance of neuston transects) were divided into eight zones over the length of the West Hawai'i coastline (Fig. 3). These zones were sectioned based on geography, bathymetry, and observed patterns over the available SAR imagery. Zones 1 and 8 represent the northern and southern ends of the island, respectively, which are frequently too windy for slicks to be visible. The slope steepens progressively moving from north to south. Zones 2 and 3 have a wide shelf and comparatively gentler slope (500 m isobath is roughly 6.5–17 km from shore); in Zone 4 the shelf drops off dramatically to a steep slope and becomes progressively steeper moving southward to where it is the steepest in Zone 7 (500 m isobath is less than 2 km from shore; see Fig. 1).

Each of the 225 SAR images was examined to note presence or absence of slick lines within each individual zone. Slicks that appeared as multiple parallel lines in series were flagged as probable internal wave slicks. Slicks that were close to and perpendicular to the shoreline but not apparently associated with any headland were flagged as likely SGD fronts. The slick presence/absence SAR data were compared to WRF wind speed data, which were interpolated to the time of each SAR image and to the centroid of each of the zones as defined by their corner points.

3. Results

3.1. Presence and frequency of slicks

The SAR images showed slick lines to be common occurrences along West Hawai'i. Some form of slick line, whether generated by internal waves, headland fronts, eddy fronts, SGD, or other mechanisms that lead to bands of smooth water or biogenic oils, was observed in more than half of all images in Zones 2–7 (Fig. 3B). Slick lines only appeared in ~25% of all images in Zones 1 and 8, however; these regions at the northern and southern ends of the island, respectively, are not fully sheltered from northeasterly trade winds by island topography as is the rest of the coastline. Comparing the observations of SAR slick lines to WRF wind speeds (Fig. 4), the slick lines appeared in over 75% of images when wind speeds were below 5 m s^{-1}. However, the appearance of slicks fell sharply to ~20% of images at wind speeds greater than 7 m s^{-1} and to less than 10% when winds surpass 10 m s^{-1}. Zones 1, 2, and 8 accounted for 94% of the noted instances of winds over 10 m s^{-1} during the times of the SAR images, while Zones 5, 6, and 7 had no instances of winds over 10 m s^{-1} during these times.

Apparent internal wave slicks were the most common type of slick line present in the SAR imagery. They were the most frequent slick type appearing in Zones 2, 4, 5, 6, and 7 and were particularly frequent along the southwestern stretch of the coastline (Fig. 3B), appearing in more

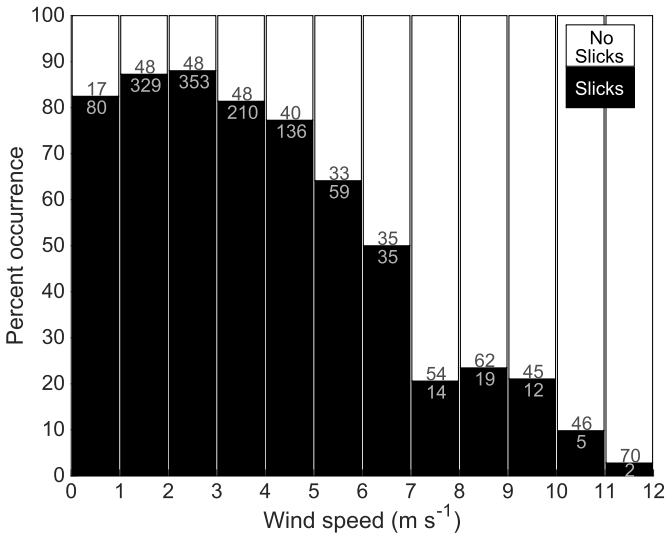

Fig. 4. Percent of SAR imagery with and without slicks by zone, binned according to Weather Research and Forecasting (WRF) wind speeds interpolated to the time of image and to the centroid of each zone (see Fig. 3). Numbers presented in each bar indicate the count of instances contributing to each percentage, where each zone on each image date is counted as a separate instance. The white bars represent no slicks present. The black bars represent slicks present.

than 50% of images in Zones 6–7. Internal wave slicks were also present in more than 24% of images in Zones 2–5, but they were only present in ~10% of images in Zones 1 and 8. Zones 1 and 8 had nearly identical (9–10%) frequency of both internal wave and SGD slicks, while in Zone 3 SGD slicks were more frequent (43% of images) than internal wave slicks (24% of images). Because the SAR images were taken multiple days apart, tracking the movement and speed of individual slick lines was not possible with SAR imagery, making it difficult to distinguish parallel lines caused by internal waves from those caused by other mechanisms such as eddies (Holt, 2004).

Internal wave slicks in the SAR image from May 24, 2017 at 6:30 p.m. HST were compared to slicks visible in time-lapse photos taken each minute between 4:50 p.m. and 6:50 p.m. HST by a Wingscapes TimeLapseCam Pro digital camera on the roof of a local homeowner (Fig. 1). Through georectification in Matlab (https://gitlasso.uqar.ca/bourda02/g_rect; Farid and Woodward, 2007; Pawlowicz, 2003) and distance measuring in ArcGIS, the slicks visible in the time-lapse photos (e.g., the labeled slick, Fig. 5) were found to be traveling an average of 0.13 m s^{-1} towards the shoreline. This corresponds with the expected velocity and orientation of internal wave slicks (Mann and Lazier, 2006). The same line can be seen in the SAR image (Fig. 5C), where it fits the criteria for categorization as a possible internal wave slick (i.e., multiple lines in parallel with bathymetry). While this does not confirm that all the possible internal wave slicks observed in the SAR images were caused by internal waves, it does suggest that it is highly likely many were. It was therefore concluded that internal waves were a significant driver of slicks observed in the region.

Mooring observations confirm the presence of internal waves *in situ*. Bottom water temperature from the T-chain moorings showed frequent cold pulses, or sudden drops in temperature, followed by more gradual warming (examples shown in Fig. 6). This is a pattern indicative of internal wave bores: Breaking internal waves drive cooler temperatures from depth up the slope into shallower, warmer ambient waters, causing a sudden drop in temperature near the bottom. This is accompanied by mixing that leads to a more gradual recovery of warmer temperatures after the bore has receded (e.g., Leichter et al., 1996). The near-surface thermistors at both moorings did not show evidence of warm fronts associated with the receding of internal wave bores. The frequency of occurrence of the internal wave bores was sporadic; intervals between cold intrusions ranged from as low as 6 min to nearly 6 h, with a median interval of 40 min. There was no apparent link between the occurrence of the cold pulses and the tidal phase, as the cold pulses were scattered with no apparent bias throughout the tidal phases as observed by comparison to the pressure time series. Auto-spectra of the temperature time series at the Kona Paradise mooring (Supplemental Fig. S3) showed a peak in high-frequency energy (95–120 cycles per day) near the surface, but no high-frequency peak near the bottom. This frequency band roughly corresponds to the ~15 min periods of internal wave slicks noted in field surveys, and the absence of the peak near the bottom implies that the internal wave bores observed at that depth were too sporadic to manifest a dominant frequency. This near-surface temperature signature was not observed at the Hōnaunau moorings, so it is unknown how robust this signal is in the region.

3.2. Description of surveyed slicks

Surveyed surface slick lines were identified as being caused by internal waves (n = 52, 65.8%), SGD (n = 9, 11.4%), tidal fronts (n = 5, 6.3%), and headland fronts (n = 2, 2.5%), and 11 (13.9%) were classified as unidentified (Fig. 7). Because slicks that appeared to be internal wave slicks in the field were prioritized in our surveys, our counts of each mechanism are not representative of the actual frequency of each mechanism. However, based on how many internal wave slicks were available for our surveys, we can say that they were a prominent generating mechanism of slicks in the region.

Near-surface (1 m depth) temperature from the CTD was compared at the inshore and offshore edges of each slick identified as an internal wave slick. Eleven of the 13 internal wave slicks for which this comparison was possible exhibited higher surface temperatures at the offshore edge of the slick than the inshore edge of the slick (temperature difference of 0.09 ± 0.03 °C mean ± standard error). This pattern likely corresponds to a slick located above the converging (downwelling) edge of an internal wave of depression propagating toward shore (Lafond, 1959); cooler water at a certain depth is followed by warmer water at the same depth as the wave trough passes.

The acoustics showed higher near-surface particulates in slicks than in ambient waters. Of the 21 slicks that had acoustics data in the 3–4 m depth bin both inside slicks and in ambient water, 17 (81.0%) displayed higher backscatter in slicks than in ambient water for that depth bin. Of those 17 slicks, 16 (76.2% of 21 total) had higher backscatter in slicks in the 4–5 m depth bin as well. The concentration factor (ratio of slick: ambient) of acoustic backscatter in 1 m depth bins and organism densities from the neuston net tows for the seven primary pair slicks are shown in Fig. 8. All measurements show higher acoustic scattering inside slicks down to 5 m depth; some show higher values in slicks at even greater depths, particularly at the north sites (Puakō and Kīholo). High values in the near-surface acoustics bins corresponded to high neuston net concentration values in the majority of the primary pair slicks (correlation between 3 and 7 m bin mean and neuston = 0.84, p-value<0.02), with the exception of the two in Miloli'i, which had the lowest values overall for both acoustic backscatter and plankton densities.

The acoustic drifter profiled three slicks that were categorized as internal wave slicks. For one of these, the drifter remained inside the slick for the entire deployment, but for the other two, the drifter profiled acoustic backscatter both inside and just outside the slick (Fig. 9). Both of these slicks showed high backscatter in a portion of the slick, though the backscatter was not uniform throughout the slicks. One slick had high backscatter down to a depth of ~4.5 m (Fig. 9A), while the other slick had high backscatter down to the deepest bin at 5.5 m (Fig. 9B), likely extending a short distance deeper than recorded. While the small sample set from the acoustic drifter cannot provide statistically significant results, it provides a picture of what the depth profile of a slick can look like along with further evidence that the accumulation in slicks may extend from the surface to as deep as 5 m or more.

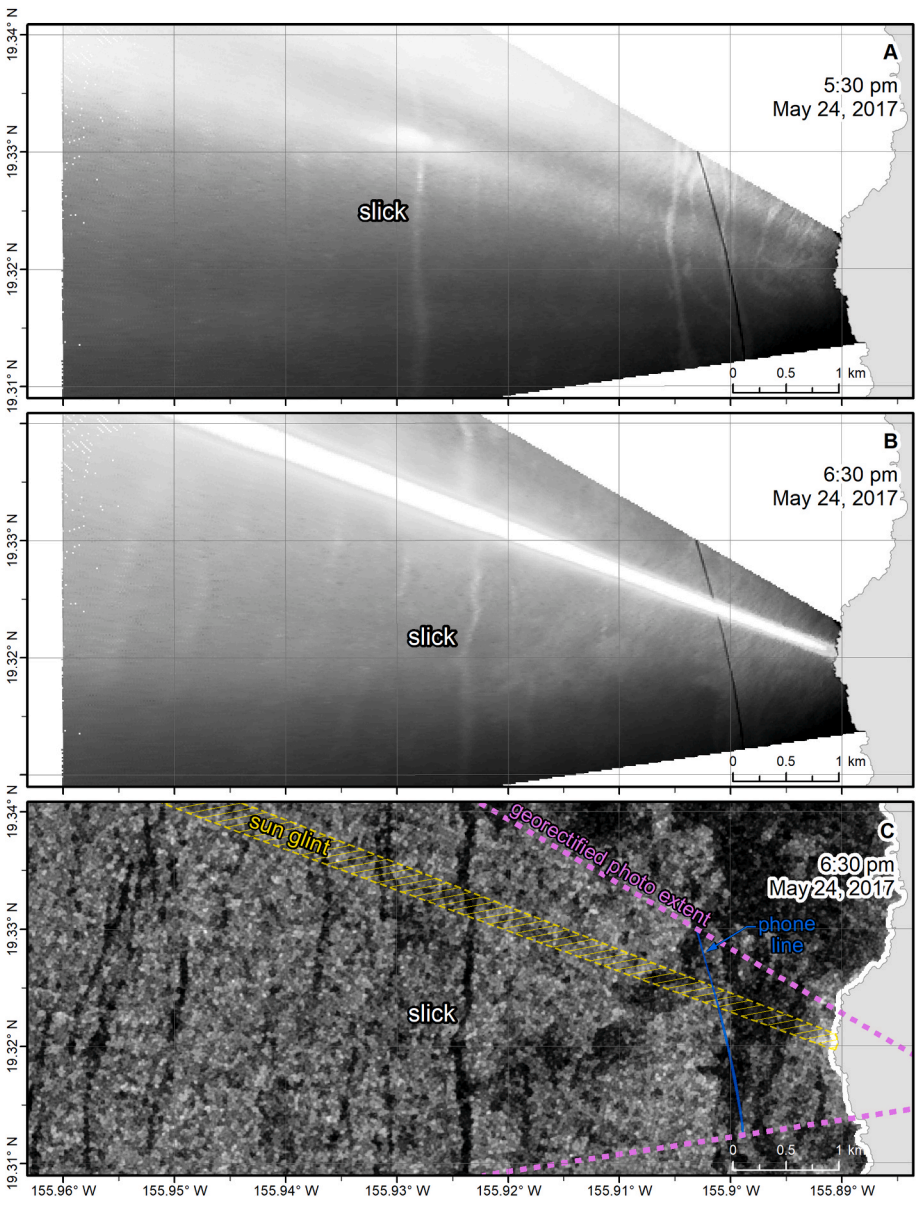

Fig. 5. Correspondence of time-lapse photos (camera location shown in Fig. 1) and SAR image highlighting shoreward progression of internal wave slicks. Georectified time-lapse photos at (A) 5:30 p.m. and (B) 6:30 p.m. HST on May 24, 2017. Black line at ~155.9°W is from a phone line across the camera's view. (C) SAR image at 6:30 p.m. HST on May 24, 2017, marked with corresponding locations of notable features in (A) and (B). One of the individual slicks visible in both the SAR image and the time-lapse photos at the same time point is labeled.

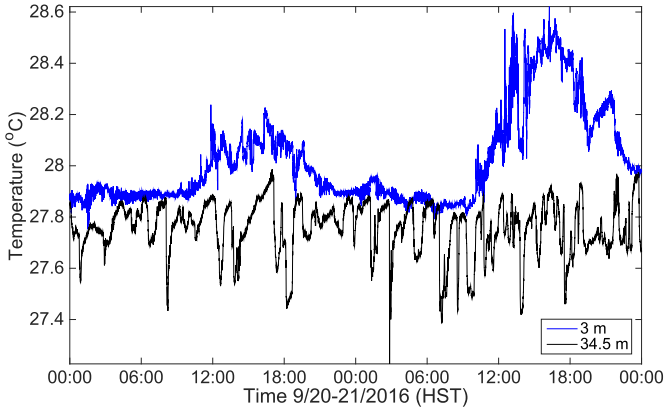

Fig. 6. Temperature measurements over time at the Hōnaunau mooring on September 20 and 21, 2016 (HST) near-surface (3 m depth, blue) and near-bottom (34.5 m depth, black). Mooring location can be seen in Fig. 1.

3.3. Accumulation by slick mechanism

Samples collected in the neuston nets were separated into four categories: zooplankton, larval invertebrates, larval fish, and plastic debris. Chlorophyll *a* (a proxy for phytoplankton biomass) collected in the bottle samples constituted a fifth category. Mean and standard error of the concentration factors (i.e., slick density/ambient density) for these categories were plotted for each generating mechanism (Fig. 10). A mean concentration factor greater than 1 indicates an enhancement inside slicks compared to ambient waters. All categories showed enhancement by each of the four identified slick-forming mechanisms.

Phytoplankton showed modest enhancement inside slicks, with mean concentration factors of 1.5, 1.1, 3.0, and 1.1 for internal wave (n = 25), SGD (n = 3), tidal (n = 2), and headland front (n = 2) slicks, respectively. One of the two tidal fronts for which chlorophyll samples were taken had an anomalously high density, leading to the high mean concentration factor. Compared to phytoplankton, enhancement of zooplankton in the slicks was greater, with mean concentration factors of 11.3, 6.2, 11.3, and 3.9 for internal wave (n = 52), SGD (n = 9), tidal (n = 5), and headland front (n = 2) slicks, respectively. For larval

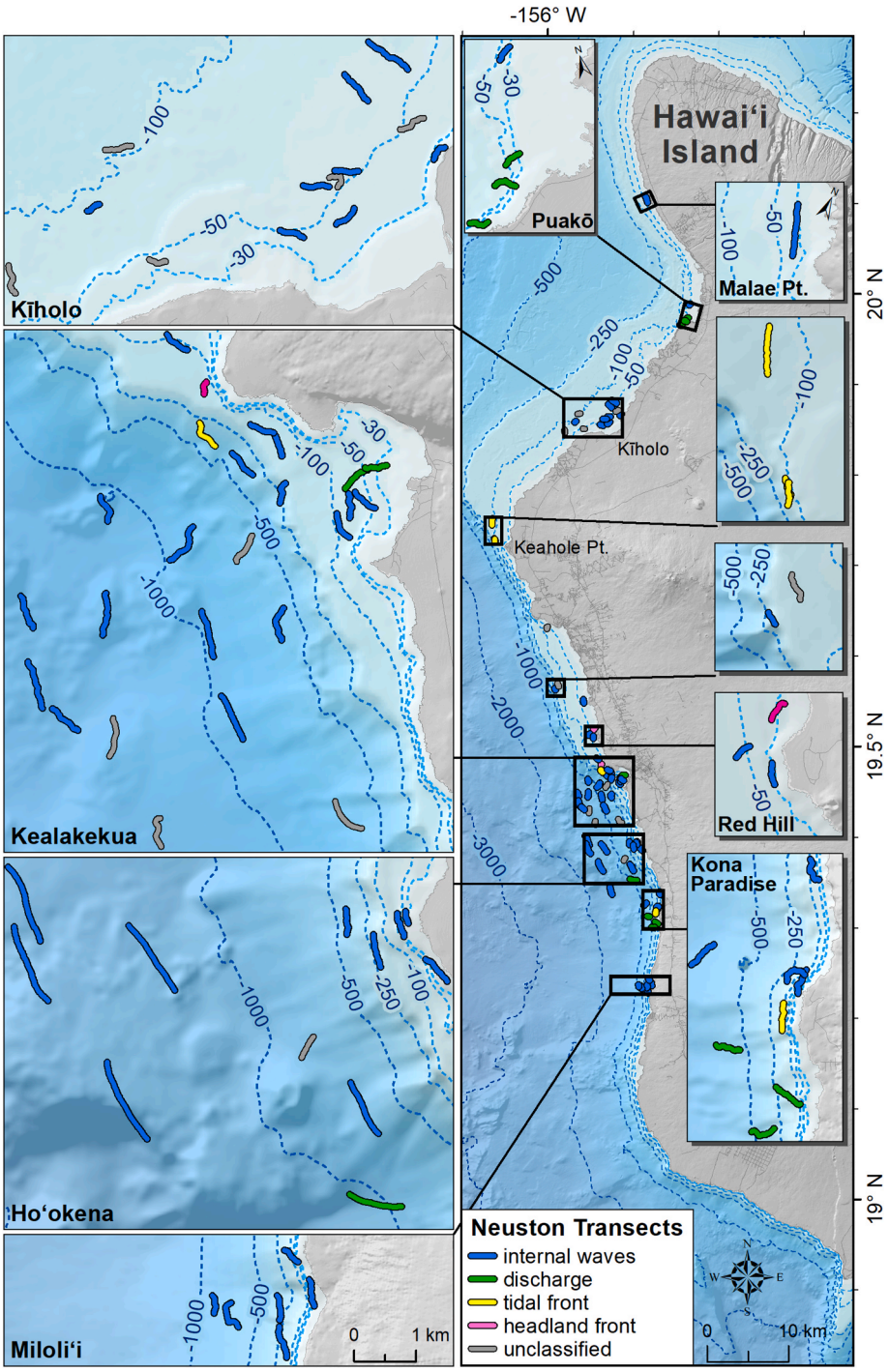

Fig. 7. Map of neuston net transects conducted in surface slicks, color-coded by designated mechanism: internal waves (n = 52, blue), submarine ground water discharge (n = 9, green), tidal front (n = 5, yellow), headland front (n = 2, pink), unclassified (n = 11, gray).

invertebrate enhancement, mean concentration factors were 21.7, 5.9, and 15.1, for internal waves (n = 52), SGD fronts (n = 9), and tidal front slicks (n = 5), respectively, but a single front with an anomalously high density of gastropod veligers brought the headland front (n = 2) mean value to 176.8. Larval fish enhancement in slicks was similar in magnitude compared to other zooplankton with mean concentration factors of 14.7, 4.0, and 3.6, for internal wave (n = 52), SGD (n = 9), and headland front (n = 2) slicks, respectively, though a single data point brought the tidal front (n = 5) mean value to 60.0 (the other four tidal fronts had values under 6.0). Plastics debris showed especially high enhancement in slicks, with mean concentration factors of 190.6, 8.8, 137.9, and 26.1, for internal wave (n = 52), SGD (n = 9), tidal front (n = 5), and headland front (n = 2) slicks, respectively.

Although tidal fronts had the highest mean concentration factors of phytoplankton and larval fish, and headland fronts had the highest mean concentration factors of larval invertebrates, the lower sample size for these mechanisms means that these values and the comparisons thereof are not as robust. The comparisons between internal wave slick and SGD front accumulation are more robust because of their larger sample sizes. Considering the mean ± standard error ranges of the concentration factors, internal wave slicks had notably greater enhancement of larval invertebrates, larval fish, and plastic debris when compared to SGD

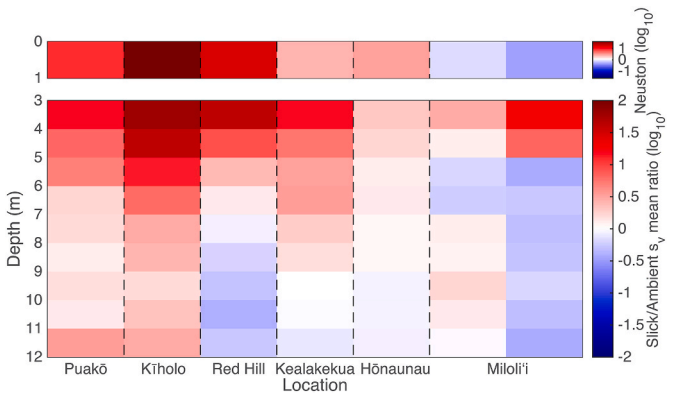

Fig. 8. In-slick/ambient water ratio for acoustics backscatter and neuston net densities of primary pair slicks. Locations are found in Figs. 1 and 7. Comparison shows correspondence between high in-slick enhancement at surface (0–1 m) as measured by the neuston tows and the near-surface depth bins measured by acoustics, with the exception of Miloli'i, which had the lowest values overall. The Puakō slick was identified as a SGD front, while all others shown here were identified as internal wave slicks. Red shades represent enhancement in the slick relative to nearby ambient water.

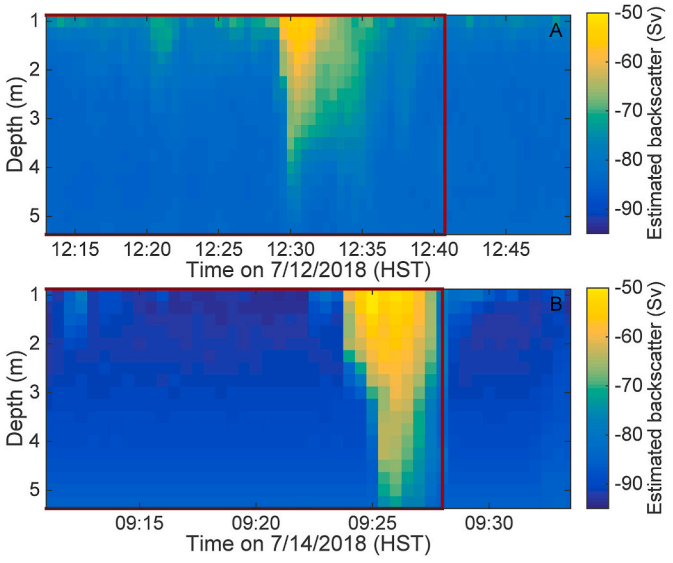

Fig. 9. Depth profiles of estimated backscatter from the acoustic drifter during two internal wave slick surveys. The drifter deployment started inside each slick and drifted outside of the surface manifestation of the slick at the time indicated by the red line.

slicks.

4. Discussion

This study identified internal wave slicks, SGD fronts, tidal fronts, and headland fronts as four distinct drivers of surface slick formation in West Hawai'i. We investigated differences in biological accumulation between these physical mechanisms and further distinguished differences in accumulation of diverse specimens, from phytoplankton to plastics. We also quantified slick occurrence at an ecosystem scale and gave evidence that wind exposure, including geographical differences in wind exposure, affect the presence of slicks. It is a common assumption that strong winds will prevent the appearance of slicks, which makes sense *a priori* and may be supported by anecdotal evidence, but to our knowledge this is the first study that explicitly confirms this relationship with a large data set (Fig. 4).

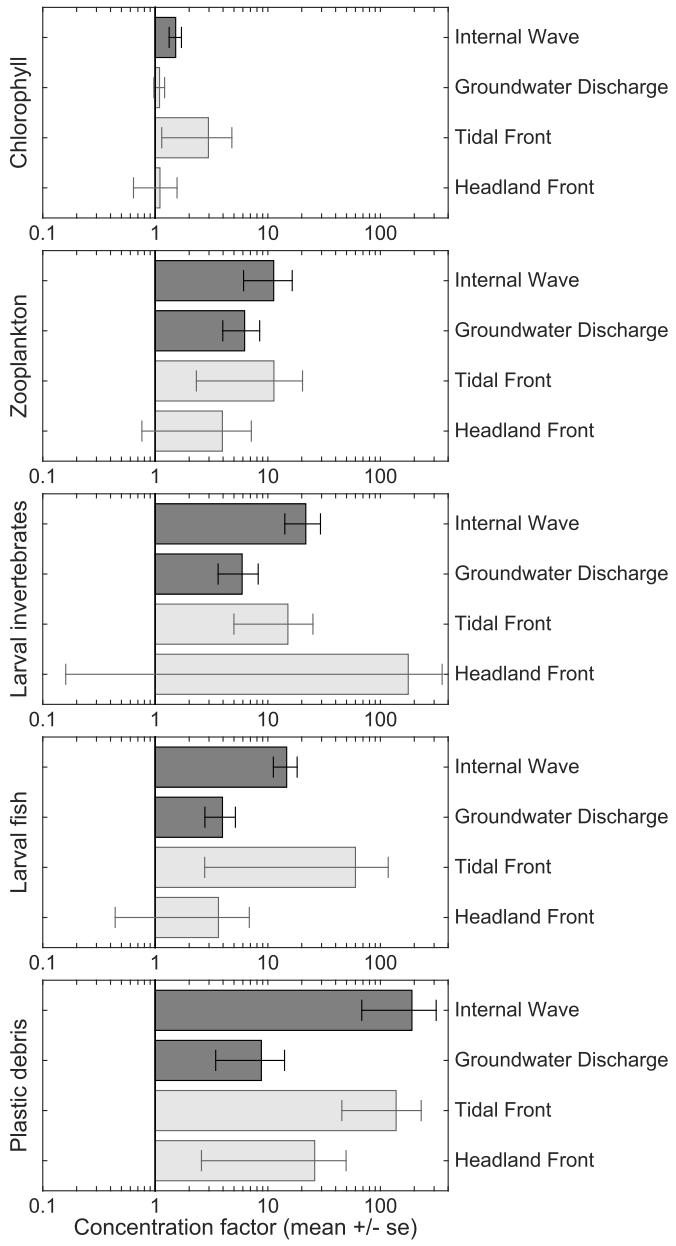

Fig. 10. Mean (filled bars, labeled with corresponding number values) and standard error (error bars) of concentration factors for chlorophyll *a*, zooplankton, larval invertebrates, larval fish, and plastic fragments for each surface slick mechanism. A concentration factor is the ratio of density in each slick tow to the density in the nearest tow in ambient water. For internal wave slicks, submarine groundwater discharge (SGD) fronts, tidal fronts, and headland fronts, respectively, sample size n = 52, 9, 5, and 2 for all variables except for chlorophyll *a*, for which n = 25, 3, 2, and 2. Because low sample size means a less robust result, values calculated using n $\leq$ 5 are displayed in a lighter shade.

Based on SAR image analysis and our surveys, internal waves were the most prominent source of slicks, followed by SGD, tidal fronts, and headland fronts. Although the two more common types of slicks (internal wave and SGD) had enhanced densities of phytoplankton, zooplankton, larval fish, larval invertebrates, and plastic debris compared to ambient waters, internal wave slicks exhibited greater enhancement than SGD slicks in all categories, with especially high accumulation of larval invertebrates, larval fish, and plastic debris (Fig. 10). We acknowledge that given the low sample size of observed tidal and headland fronts, these results should be viewed with caution.

Still, the five tidal fronts we sampled had high accumulation values on par with internal wave slicks, illustrating that these merit further study.

Spatial characteristics of the different slick drivers may affect their ecological impact. Headland and SGD fronts occur close to shore (10s–100s of meters) and accumulate less intensely than internal wave slicks and tidal front slicks (Fig. 10), which operate farther offshore (100s of meters to kilometers). Pelagic larvae of demersal fishes and invertebrates are expected to avoid the shoreline and thus to be found farther offshore until competency is reached (Pineda, 2000; Leis and McCormick, 2002), which could explain the relatively low accumulation of larvae in the more inshore SGD and headland fronts. Internal wave slicks can accumulate a wide variety of animals and debris over a broad swath of the surface ocean as they propagate from slope waters toward shore (Shanks, 1983, 1988; Kingsford and Choat, 1986), and they are regular yet ephemeral features. Tidal fronts are more stationary, occurring along a particular isobath depending on current and mixing conditions (Mann and Lazier, 2006), and thus could offer a more predictable habitat for larger, more competent larval fish to target (as suggested for larval billfish in West, 2004). Based on these data, we postulate that internal wave and tidal front slicks have a greater ecological impact on the base of the food chain (phytoplankton to larval fish) than headland and SGD fronts. For internal wave slicks, the biological accumulation combined with high rates of occurrence suggest they are important nursery habitat for neustonic larval fish and invertebrates in this region (see also Whitney et al., 2021). However, the coincidence of strikingly high accumulations of plastic debris (191x concentration factor) and larval fish (15x concentration factor) in internal wave slick habitats has presumably adverse consequences for the marine ecosystems and fisheries of Hawai'i, such as increased ingestion of microplastics by fish larvae (Gove et al., 2019).

The accumulation of neustonic larvae in internal wave slicks has previously been observed in a variety of temperate regions around the world (e.g., Kingsford and Choat, 1986; Shanks, 1983; Shanks, 1988; Weidberg, 2014). The magnitude of larval fish accumulation in slicks seen in our study (concentration factor of 14.7x) is comparable to what has been measured in temperate waters (e.g., 12.5x in Kingsford and Choat, 1986; and 24.5x in Shanks, 1983). In shallow waters (<20 m), surface accumulation of larvae and zooplankton has also been attributed to warm fronts associated with internal wave bores (e.g., Pineda, 1991, 1994; Vargas et al., 2004; Walter et al., 2012). While the nonlinearity of internal wave bores and their associated fronts allow for the transport of materials toward shore, the theoretical linearity of internal wave slicks means the same materials would tend to be accumulated and dispersed in sequence as the respective convergent and divergent sections of the wave pass by, analogous to how an idealized linear wave travels without transporting any water (Pineda, 1994; Mann and Lazier, 2006). In reality, some degree of nonlinearity allows materials to be transported with internal wave slicks, but the transport is less significant than that of internal wave bores (Franks et al., 2020; Shanks et al., 1983). This distinction (more vs. less transport) is relevant to the potential ecological impact of the slicks, which includes transport of larvae and nutrients (e.g., Leichter et al., 1996; Pineda 1994). Our mooring data (Fig. 6) indicate that there were internal wave bores along a portion of West Hawai'i at 35–45 m depth. The temperature changes caused by these bores were indicative of water transported from depths no deeper than 90 m, and they were usually confined to the bottom 10 m. The internal wave bores at this depth range were not accompanied by temperature signatures at the surface that would be associated with particle-transporting surface warm fronts (Pineda, 1994). If such warm fronts associated with internal wave bores do form in this region, they would likely be in shallower water than these moorings. Of the internal wave slicks that we surveyed, 87% were in depths >40 m; 56% were in depths >100 m. Therefore, although the hydrographic data we have for the slicks are not sufficient to determine whether each one is caused by an internal wave bore or (mostly linear) internal wave slick, we can infer that the overwhelming majority, being located in deep water, are the latter. Interestingly, even if the internal wave slicks do not cause bulk transport of materials, competent swimmers including larval fish may choose to stay in moving slick habitat and purposely travel with the slick bands (i.e., follow the convergent portion of the traveling wave) toward shore (Shanks, 1988; Kingsford and Choat, 1986; Whitney et al., 2021).

The accumulation of materials in the smooth internal wave slicks indicates that these slicks are forming over the part of the internal wave associated with surface convergence. Seemingly conflicting explanations of internal wave slicks place the smooth slicks over regions of both surface convergence (e.g., Curtin and Mooers, 1975; Ewing, 1950; Mann and Lazier, 2006) and, alternatively, surface divergence (e.g., Artale et al., 1990; Osborne et al., 1978; Woodson, 2018). In fact, smooth bands may form in either location based on the dominance of one of two effects: (1) straining, which causes ripples in surface convergent regions and smoothness in surface divergent regions, and (2) the suppression of surface ripples by a surfactant film and/or other materials that accumulate in convergent regions (Baines, 1981; da Silva, 1998). The fact that buoyant, passive materials (e.g., plastics) accumulated in the observed internal wave slicks points to the dominance of the surfactant film effect over the straining effect in this study, and this explanation is further supported by both field and SAR observations of slicks in the region. Throughout this study, parallel bands of smoother-than-baseline water were observed, but parallel bands of rougher-than-baseline water were not seen. The latter would be expected to alternate with smooth slicks in cases where straining was responsible for the slick pattern, but it would not be expected in cases where surfactant films suppress ripples in regions of surface convergent flows (da Silva, 1998).

Internal wave slicks had high accumulations of zooplankton, larval fish, and larval invertebrates, and their prominence as habitat for these animals in the region is reinforced by their expansive spatial coverage and high temporal frequency. SAR data presented here highlight that slicks are present along much of the coastline for the majority of the year (Fig. 3B). In regards to three-dimensional volume of habitat provided by the slicks, acoustic backscatter profiles indicate that accumulation is generally enhanced in the slicks down to depths of 5 m or more, giving a greater volume of potential biological impact than a strictly surface feature would provide. More observations are needed to capture the variation in depth and surface area coverage in various ocean conditions over time. However, it is clear that slicks are common and prevalent surface features along this coastline with significant ecological impacts to the base of the marine ecosystem.

5. Conclusions

Internal waves are ubiquitous features in the world's oceans (Munk and Wunsch, 1998), and slicks have been observed in many continental and island coastal systems around the world, from the Bay of Biscay (Weidberg et al., 2014) to the Andaman Sea (Osborne et al., 1978) to coastal California (Shanks, 1983). Zooplankton and neustonic larvae have previously been observed to accumulate in internal wave slicks (e.g., Shanks, 1983; Kingsford and Choat, 1986; Weidberg et al., 2014). This study shows the prominence of internal wave slicks as accumulators of larval fish, larval invertebrates, and plastics as compared to slicks caused by other physical mechanisms. Moreover, we provide evidence that internal wave slicks are common and prevalent surface features in this region. This study also demonstrates the potential of internal wave slicks both to be an important component of the ecosystem as larval fish habitat and to introduce negative ecosystem effects through the accumulation of plastics. Further study could help to elucidate the accumulative effects of tidal fronts and headland fronts, but based on frequency and observed accumulation, internal wave slicks appear to be more important components of this ecosystem than slicks generated by other mechanisms. The Hawaiian Ridge is a known hotspot for internal wave generation (e.g., Merrifield et al., 2001; Merrifield and Holloway, 2002; Rudnick et al., 2003), and internal waves may therefore be a more dominant mechanism for slick formation in this region than elsewhere.

However, given the evidence that all slicks sampled in this region not only provided larval fish nursery habitat but also accumulated plastics, further study of the ecosystem impacts of slicks on larvae and plastics is merited in other regions worldwide.

Declaration of competing interest

The authors declare that they have no known competing financial interests or personal relationships that could have appeared to influence the work reported in this paper.

Acknowledgments

We would like to thank Mark Merrifield, Doug Luther, Jeffrey Polovina, and Jeff Hare for supporting this work. We also thank the crew of NOAA Ship *Oscar Elton Sette*, and the DLNR Division of Boating and Ocean Recreation, Honokōhau Small Boat Harbor, for the use of their vessel. We are very grateful for the two anonymous reviewers whose insightful comments have significantly improved this work. Special thanks to John and Sue Kellam for their help with slick imaging. Some elements of Fig. 2 are courtesy of the Integration and Application Network, University of Maryland Center for Environmental Science (ian.umces.edu/symbols/). This research was supported by the Joint Institute for Marine and Atmospheric Research, NOAA's West Hawai'i Integrated Ecosystem Assessment (contribution no. 2021_1), NOAA's Fisheries and the Environment program, and NOAA's Pacific Islands Fisheries Science Center.

Appendix A. Supplementary data

Supplementary data to this article can be found online at https://doi.org/10.1016/j.csr.2021.104558.

References

Aron, W., 1962. The distribution of animals in the eastern North Pacific and its relationship to physical and chemical conditions. Journal of the Fisheries Board of Canada 19, 271–314.
Artale, V., Levi, D., Marullo, S., Santoleri, R., 1990. Analysis of nonlinear internal waves observed by Landsat thematic mapper of messina. J. Geophys. Res. 95, 16065–16073.
Baines, P.G., 1981. Satellite observations of internal waves on the Australian north-west shelf. Aust. J. Mar. Freshw. Res. 32, 457–463.
Brown, D., Cheng, L., 1981. New net for sampling the ocean surface. Mar. Ecol. Prog. Ser. 5, 224–227.
Curtin, T.B., Mooers, C.N.K., 1975. Observation and interpretation of a high-frequency internal wave packet and surface slick pattern. J. Geophys. Res. 80, 882–894.
da Silva, J.C.B., Ermakov, S.A., Robinson, I.S., Jeans, D.R.G., Kijashko, S.V., 1998. Role of surface films in ERS SAR signatures of internal waves on the shelf: 1. Short-period internal waves. J. Geophys. Res. 103, 8009–8031.
De Robertis, A., Higginbottom, I., 2007. A post-processing technique to estimate the signal-to-noise ratio 504 and remove echosounder background noise. ICES (Int. Counc. Explor. Sea) J. Mar. Sci. 64 (6), 1282–1291.
Deines, K., 1999. Backscatter estimation using broadband Acoustic Doppler current profilers. In: Proc. Sixth Working Conf. On Current Measurement. IEEE, San Diego, CA, pp. 249–253.
Demer, D.A., Berger, L., Bernasconi, M., Bethke, E., Boswell, K., Chu, D., et al., 2015. Calibration of acoustic 498 instruments. ICES (Int. Counc. Explor. Sea) Coop. Res. Rep. 326, 1–133.
DiGiacomo, P.M., Holt, B., 2001. Satellite observations of small coastal ocean eddies in the Southern California Bight. J. Geophys. Res. 106, 22521–22543.
Echoview Software Pty. Ltd, 2017. Echoview Software. Echoview Software Pty. Ltd., Australia. Hobart, 502, version 8.0.
Ewing, G., 1950. Slicks, surface films, and internal waves. J. Mar. Res. 9, 161–187.
Farid, H., Woodward, J.B., 2007. Video Stabilization and Enhancement. Dartmouth College, Hanover, NH.
Foote, K.G., Vestnes, G., Maclennan, D.N., Simmonds, E.J., 1987. Calibration of acoustic instruments for fish density estimation: a practical guide. ICES (Int. Counc. Explor. Sea) Coop. Res. Rep. 144, 1–81.
Franks, P.J.S., 1997. Spatial patterns in dense algal blooms. Limnol. Oceanogr. 42 (5), 1297–1305.
Franks, P.J., Garwood, J.C., Ouimet, M., Cortes, J., Musgrave, R.C., Lucas, A.J., 2020. Stokes drift of plankton in linear internal waves: cross-shore transport of neutrally buoyant and depth-keeping organisms. Limnol. Oceanogr. 65, 1286–1296.
Gorelick, N., Hancher, M., Dixon, M., Ilyushchenko, S., Thau, D., Moore, R., 2017. Google Earth engine: planetary-scale geospatial analysis for everyone. Rem. Sens. Environ.
Gove, J.M., Whitney, J.L., McManus, M.A., Lecky, J., Carvalho, F.C., Lynch, J.M., Li, J., Neubauer, P., Smith, K.A., Phipps, J.E., Kobayashi, D.R., Balagso, K.B., Contreras, E. A., Manuel, M.E., Merrifield, M.A., Polovina, J.J., Asner, G.P., Maynard, J.A., Williams, G.J., 2019. Prey-sized plastics are invading larval fish nurseries. Proc. Natl. Acad. Sci. Unit. States Am. 116 (48), 24143–24149.
Gove, J.M., McManus, M.A., Neuheimer, A.B., Polovina, J.J., Drazen, J.C., Smith, C.R., Merrifield, M.A., Friedlander, A.M., Ehses, J.S., Young, C.W., Dillon, A.K., Williams, G.J., 2016. Near-island biological hotspots in barren ocean basins. Nat. Commun. 7, 1–8.
Holt, B., 2004. SAR imaging of the ocean surface, 464. In: Jackson, C.R., Apel, J.R. (Eds.), Synthetic Aperture Radar Marine User's Manual. NOAA, Washington, D.C., USA, pp. 25–79. U.S. Dept. of Commerce.
Hsu, M., Liu, A.K., Liu, C., 2000. A study of internal waves in the China Seas and Yellow Sea using SAR. Continent. Shelf Res. 20, 389–410.
Isaacs, J., 1953. Isaccs-Kidd mid-water trawl final report. SIO Oceanographic Equipment Report 1, 1–21.
Johnson, A.G., 2008. Groundwater Discharge from the Leeward Half of the Big Island. M. S. thesis. Univ. of Hawaii, Hawaii.
Johnson, A.G., Glenn, C.R., Burnett, W.C., Peterson, R.N., Lucey, P.G., 2008. Aerial infrared imaging reveals large nutrient-rich groundwater inputs to the ocean. Geophys. Res. Lett. 35, L15606. https://doi.org/10.1029/2008GL034574.
Kay, E.A., Lau, L.S., Stroup, E.D., Dollar, S.J., Fellows, D.P., Young, R.H.F., 1977. Hydrologic and Ecological Inventory of Coastal Waters of West Hawaii. Univ. of Hawaii. Technical Report No. 105. Water Resources Center.
Kingsford, M.J., Choat, J.H., 1986. Influence of surface slicks on the distribution and onshore movement of small fish. Mar. Biol. 91, 161–171.
Kingsford, M.J., Wolanski, E., Choat, J.H., 1991. Influence of tidally induced fronts and Langmuir circulation on distribution and movements of presettlement fishes around a coral reef. Mar. Biol. 109, 167–180. https://doi.org/10.1007/BF01320244.
Kingsford, M.J., 1990. Linear oceanographic features: a focus for research on recruitment processes. Aust. J. Ecol. 15, 391–401.
Lafond, E.C., 1959. Slicks and temperature structure in the sea. Nav. Electron. Lab., Rep. 937, 1–27 (San Diego, California).
Leichter, J.J., Wing, S.R., Miller, S.L., Denny, M.W., 1996. Pulsed delivery of subthermocline water to Conch Reef (Florida Keys) by internal tidal bores. Limnol. Oceanogr. 41 (7), 1490–1501.
Leichter, J.J., Shellenbarger, G., Genovese, S.J., Wing, S.R., 1998. Breaking internal waves on a Florida (USA) coral reef: a plankton pump at work? Mar. Ecol. Prog. Ser. 166, 83–97.
Leis, J.M., McCormick, M.I., 2002. The biology, behavior, and ecology of the pelagic, larval stage of coral reef fishes. In: Sale, P.F. (Ed.), Coral Reef Fishes: Dynamics and Diversity in a Complex Ecosystem. Academic Press, Cambridge, pp. 171–199.
Mann, K.H., Lazier, J.R., 2006. Dynamics of Marine Ecosystems: Biological-Physical Interactions in the Oceans. Blackwell Publishing, Cambridge, p. 512.
Marmorino, G.O., Smith, G.B., V Toporkov, J., Sletten, M.A., Perkovic, D., Frasier, S.J., 2008. Evolution of ocean slicks under a rising wind. J. Geophys. Res. 113, C04030.
Mattos, H., Mujica, A., 2012. Surface zooplankton composition in slick and rough zones in Coquimbo Bay (November 2001). Lat. Am. J. Aquat. Res. 40, 453–461.
Merrifield, M.A., Holloway, P.E., 2002. Model estimates of M2 internal tide energetics at the Hawaiian Ridge. J. Geophys. Res. 107, 1–12.
Merrifield, M.A., Holloway, P.E., Johnston, T.M.S., 2001. The generation of internal tides at the Hawaiian Ridge. Geophys. Res. Lett. 28, 559.
Morgan, S.G., Fisher, J.L., Largier, J., 2011. Larval retention, entrainment, and accumulation in the lee of a small headland. Limnol. Oceanogr. 56, 161–178, 10.4319/lo.2011.56.1.0161.
Mullarney, J.C., Henderson, S.M., 2013. A novel drifter designed for use with a mounted Acoustic Doppler Current Profiler in shallow environments. Limnol Oceanogr. Methods 11, 438–449.
Mullison, J., 2017. Backscatter estimation using broadband Acoustic Doppler current profilers. In: ASCE Hydraulic Measurements & Experimental Methods Conference. Durham, NH. July 9–12, 2017.
Munk, W., Wunsch, C., 1998. Abyssal recipes II: energetics of tidal and wind mixing. Deep-Sea Res. Part I Oceanogr. Res. Pap. 45, 1977–2010.
Munk, W.H., Armi, L., Fischer, K., Zachariasen, F., 2000. Spirals on the sea. Proc. Roy. Soc. Lond. A 456, 1217–1280.
Osborne, A.R., Burch, T.L., Scarlet, R.I., 1978. The influence of internal waves on deep-water drilling. J. Petrol. Technol. 30, 1497–1504.
Pawlowicz, R., 2003. Quantitative visualization of geophysical flows using low-cost oblique digital time-lapse imaging. IEEE J. Ocean. Eng. 28, 699–710.
Peterson, R.N., Burnett, W.C., Glenn, C.R., Johnson, A.J., 2007. A box model to quantify groundwater discharge along the Kona coast of Hawaii using natural tracers. In: Sanford, W., Langevin, C., Polemio, M., Povinec, P. (Eds.), A New Focus on Groundwater-Seawater Interactions. International Association of Hydrological Sciences Press, London, pp. 142–149.
Pineda, J., 1991. Predictable upwelling and the shoreward transport of planktonic larvae by internal tidal bores. Science 253, 548–551.
Pineda, J., 1994. Internal tidal bores in the nearshore: warm-water fronts, seaward gravity currents and the onshore transport of neustonic larvae. J. Mar. Res. 52, 427–458.
Pineda, J., 2000. Linking larval settlement to larval transport: assumptions, potentials, and pitfalls. Oceanography of the Eastern Pacific I 84–105.

Reid, S.B., Hirota, J., Young, R.E., Hallacher, L.E., 1991. Mesopelagic-boundary community in Hawaii: micronekton at the interface between neritic and oceanic ecosystems. Mar. Biol. 109, 427–440.
Roughgarden, J., Pennington, J.T., Stoner, D., Alexander, S., Miller, K., 1991. Collisions of upwelling fronts with the intertidal zone: the cause of recruitment pulses in barnacle populations of central California. Acta Oecol. 12, 35–51.
Rudnick, D.L., Boyd, T.J., Brainard, R.E., Carter, G.S., Gary, D., Gregg, M.C., Holloway, P. E., Klymak, J.M., Kunze, E., Lee, C.M., Levine, M.D., Luther, D.S., Martin, J.P., Merrifield, M.A., Moum, J.N., Nash, J.D., Pinkel, R., Rainville, L., Sanford, T.B., Egbert, G.D., 2003. From tides to mixing along the Hawaiian ridge. Science 84 301, 355–357.
Ryan, J.P., Fischer, A.M., Kudela, R.M., McManus, M.A., Myers, J.S., Paduan, J.D., Ruhsam, C.M., Woodson, C.B., Zhang, Y., 2010. Recurrent frontal slicks of a coastal ocean upwelling shadow. J. Geophys. Res. 115, 1–15.
Schneider, C.A., Rasband, W.S., Eliceiri, K.W., 2012. NIH Image to ImageJ: 25 years of image analysis. Nat. Methods 9, 671. https://doi.org/10.1038/nmeth.2089.
Shanks, A., 1983. Surface slicks associated with tidally forced internal waves may transport pelagic larvae of benthic invertebrates and fishes shoreward. Mar. Ecol. Prog. Ser. 13, 311–315.
Shanks, A.L., 1988. Further support for the hypothesis that internal waves can cause shoreward transport of larval invertebrates and fish. Fish. Bull. 86, 703–714.
Shanks, A.L., 1995. Orientated swimming by megalopae of several eastern North Pacific crab species and its potential role in their onshore migration. J. Exp. Mar. Biol. Ecol. 186, 1–16.
Simmonds, J., MacLennan, D.N., 2005. Fisheries Acoustics: Theory and Practice, second ed. Blackwell Publishing, Oxford, p. 456.
Vargas, C.A., Narváez, D.A., Piñonez, A., Venegas, R., Navarrete, S.A., 2004. Internal tidal bore warm fronts and settlement of invertebrates in Central Chile. Estuar. Coast Shelf Sci. 61, 603–612. https://doi.org/10.1016/j.ecss.2004.07.006.
Walter, R.K., Woodson, C.B., Arthur, R.S., Fringer, O.B., Monismith, S.G., 2012. Nearshore internal bores and turbulent mixing in southern Monterey Bay. J. Geophys. Res. 117 (C7), C07017.
Weidberg, N., Lobón, C., López, E., García Flórez, L., Fernández Rueda, M. del P., Largier, J.L., Acuña, J.L., 2014. Effect of nearshore surface slicks on meroplankton distribution: role of larval behaviour. Mar. Ecol. Prog. Ser. 506, 15–30.
West, A.P., 2004. Aspects of the Early Life History of Billfish off Kona. Hawaii. Dissertation, University of Technology, Sydney.
Whitney, J.L., Gove, J.M., McManus, M.A., Lecky, J., Smith, K.A., Neubauer, P., Phipps, J.E., Contreras, E.A., Kobayashi, D.R., Asner, G.P., 2021. Surface slicks are pelagic nurseries for diverse ocean fauna. Sci. Rep. 11. Article 3197.
Woodson, C.B., McManus, M.A., 2007. Foraging behavior can influence dispersal of marine organisms. Limnol. Oceanogr. 56, 2701–2709.
Woodson, C.B., 2018. The Fate and Impact of Internal Waves in Nearshore Ecosystems. Annu. Rev. Mar. Sci. 10, 421–441. https://www.annualreviews.org/doi/10.1146/annurev-marine-121916-063619.
Woodson, C.B., McManus, M.A., Tyburczy, J.A., Barth, J.A., Washburn, L., Caselle, J.E., Carr, M.H., Malone, D.P., Raimondi, P.T., Menge, B.A., Palumbi, S.R., 2012. Coastal fronts set recruitment and connectivity patterns across multiple taxa. Limnol. Oceanogr. 57 (2), 582–596. https://doi.org/10.4319/lo.2012.57.2.0582.
Young, M., Adams, N.J., 2010. Plastic debris and seabird presence in the Hauraki Gulf, New Zealand. N. Z. J. Mar. Freshw. Res. 44, 167–175.